Nuclear Engineering and Technology 50 (2018) 937–943

Contents lists available at ScienceDirect

Nuclear Engineering and Technology

journal homepage: www.elsevier.com/locate/net

Original Article

Dosimetric characterization and commissioning of a superficial electronic brachytherapy device for skin cancer treatment

Han Beom Park [a], Hyun Nam Kim [a], Ju Hyuk Lee [a], Ik Jae Lee [b], Jinhyun Choi [b], Sung Oh Cho [a, *]

[a] Department of Nuclear and Quantum Engineering, Korea Advanced Institute of Science and Technology, 373-1 Guseong, Yuseong, Daejeon 305-701, South Korea
[b] Department of Radiation Oncology, Gangnam Severance Hospital, Yonsei University College of Medicine, Seoul 146-92, South Korea

ARTICLE INFO

Article history:
Received 12 January 2018
Received in revised form
29 March 2018
Accepted 4 April 2018
Available online 12 April 2018

Keywords:
Carbon Nanotube
Electronic Brachytherapy
Miniature X-ray Tube
Radiotherapy Experiments
Skin Cancer

ABSTRACT

Background: This work presents the performance of a novel electronic brachytherapy (EBT) device and radiotherapy (RT) experiments on both skin cancer cells and animals using the device.
Methods and materials: The performance of the EBT device was evaluated by measuring and analyzing the dosimetric characteristics of X-rays generated from the device. The apoptosis of skin cancer cells was analyzed using B16F10 melanoma cancer cells. Animal experiments were performed using C57BL/6 mice.
Results: The X-ray characteristics of the EBT device satisfied the accepted tolerance level for RT. The results of the RT experiments on the skin cancer cells show that a significant apoptosis induction occurred after irradiation with 50 kVp X-rays generated from the EBT device. Furthermore, the results of the animal RT experiments demonstrate that the superficial X-rays significantly delay the tumor growth and that the tumor growth delay induced by irradiation with low-energy X-rays was almost the same as that induced by irradiation with a high-energy electron beam.
Conclusions: The developed new EBT device has almost the same therapeutic effect on the skin cancer with a conventional linear accelerator. Consequently, the EBT device can be practically used for human skin cancer treatment in the near future.

1. Introduction

The incidence of skin cancers is constantly increasing [1,2]. Several options are available to treat skin cancers, such as simple surgery [3], Mohs surgery [4], chemotherapy [5], cryotherapy [6], photo dynamic therapy [7], and radiotherapy (RT) [8–11]. Among the available options, RT is a favored procedure particularly for patients who have difficulty in undergoing surgery because of aging and who do not want to develop cosmetic defects from surgery.

RT for skin cancers includes external RT and brachytherapy. External RT uses a megavolt electron beam as a radiation source and, thus, requires a high-cost linear accelerator facility and large space for the installation and radiation shielding [12]. Furthermore, external RT has a problem related to local radiation borders. Brachytherapy using radionuclides such as Ir-192 and Re-188 is another option [13]. However, radionuclide-based brachytherapy has a few disadvantages: constant production of radiation, fixed radiation energy, and difficulty in storage and management of the radionuclides. An alternative RT to overcome these drawbacks is electronic brachytherapy (EBT) based on a superficial X-ray (<100 kVp) tube. On/off controllable X-ray production, variation of X-ray energy, minimal shielding requirements, and low cost are the advantages of using the EBT. At present, a few electronic brachytherapy systems, such as Xoft Axxent [14], Intrabeam [15,16], and Esteya [17] devices, have been commercialized.

Recently, we have developed a novel EBT device. In this study, we characterized the performance of the new EBT device and conducted commissioning tests on both cells and animals to examine the therapeutic effect of the device on skin cancers.

2. Methods and materials

2.1. The superficial EBT device

The developed EBT device is shown in Fig. 1A. One of the main features of the EBT device is that a miniature X-ray tube [18] operating with a carbon nanotube (CNT) field emitter was used as an

* Corresponding author.
E-mail address: socho@kaist.ac.kr (S.O. Cho).

https://doi.org/10.1016/j.net.2018.04.007

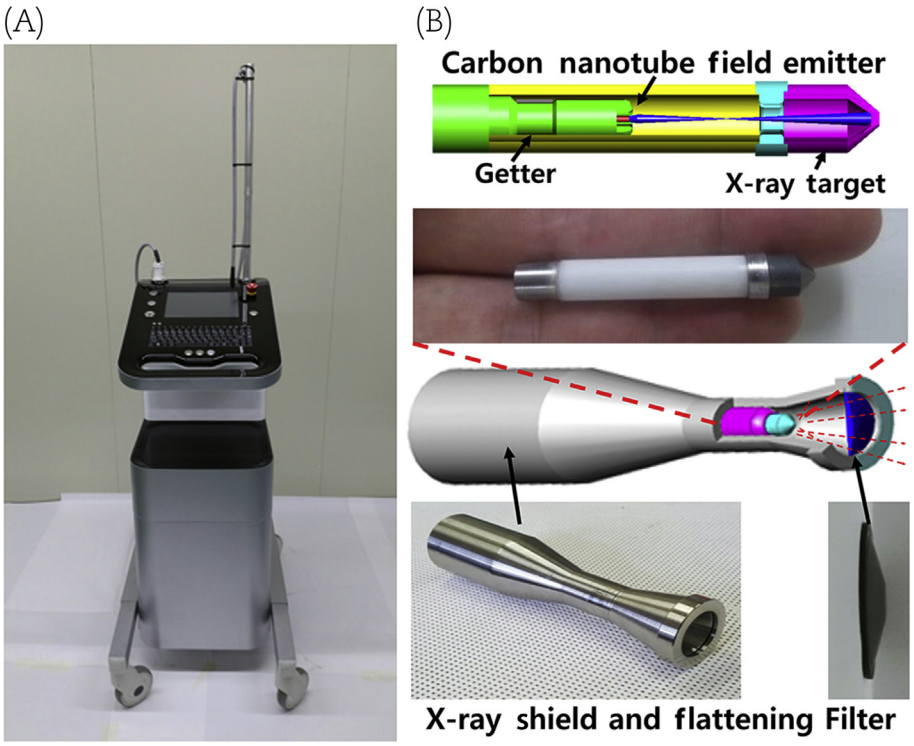

Fig. 1. The developed EBT device. (A) Full assembly photo. (B) Schematic drawing and photo of the treatment unit in the EBT device. EBT, electronic brachytherapy.

X-ray source of the device. The miniature X-ray tube has an outer diameter of 7 mm and a length of 47 mm and is normally operated at 50 kVp. X-rays are generated from a transmission-type X-ray target. The miniature X-ray tube is wrapped with a surface applicator (Fig. 1B). The surface applicator consists of an X-ray shield (2-mm–thick stainless steel) and a conical-shaped graphite flattening filter. The miniature X-ray tube equipped with the surface applicator produces spatially uniform X-rays over the desired skin region while almost completely shielding X-rays outside of the region.

2.2. Evaluations of the EBT device performance

2.2.1. X-ray spatial distribution

To investigate whether the EBT device is suitable for skin cancer treatment, X-ray dosimetric characteristics such as flatness, symmetry, and penumbra were evaluated. The three parameters were characterized by analyzing the X-ray spatial dose distribution following the definitions in the International Electrotechnical Commission 60976 criteria [19]. The X-ray spatial dose distribution was measured using a radiochromic film (Gafchromic EBT3 film; International Specialty Products, USA), which has a color-changing property when irradiated with X-rays. After scanning the irradiated films with a scanner (Epson 11000XL; Seiko Epson Corp., Japan), dose distribution was obtained by analyzing the red channel values in the scanned image. For the calibration of the film dose, the variation of the red channel value as a function of X-ray dose was premeasured using the miniature X-ray tube and a soft X-ray parallel-plate ionization chamber (PTW T34013; PTW Freiburg GmbH, Freiburg, Germany). The film dose measurements were carried out following the American Association of Physicists in Medicine (AAPM) TG-55 protocol [20].

2.2.2. Half value layer

Half value layers (HVLs) of the generated X-rays were measured to identify the absorbed doses at the skin surface. Measurement of the HVL was conducted following the TG-61 protocol [21]. For the HVL measurement, high-purity (>99.9 %) aluminum (Al) slabs of varying thicknesses ranging from 0.1 mm to 1.0 mm, Al foils with 18 μm thickness, and an ionization chamber (PTW T34013) were used. The distance between the X-ray tube and ionization chamber was 25 cm, and the Al attenuation materials were placed at the middle position between the tube and ion chamber. The HVL values were obtained through measuring the air kerma rates of X-rays passing through the Al materials by changing the thickness of the materials. The air kerma rates were determined by averaging five results measured with the ionization chamber.

2.2.3. Absorbed dose rate at the skin surface

The absorbed dose rate at the skin surface was identified following the in-air method in the AAPM TG-61 protocol [21]. First, the absorbed dose at the water surface is given by

$$D_{w,z=0} = MN_K B_w P_{stem,air} \left[(\overline{\mu}_{en}/\rho)^w_{air}\right]_{air}, \quad (1)$$

where M is the corrected reading value of the ionization chamber and N_K is air kerma calibration factor. M value was measured using an ionization chamber (PTW T34013). N_K value was provided by the PTW laboratory and adjusted through the measurement of HVL. Backscatter factor B_w and mass energy coefficient ratio of water to air $[(\overline{\mu}_{en}/\rho)^w_{air}]_{air}$ were determined from the Table 1 of TG-61 protocol. $P_{stem,air}$, chamber stem correction factor, is normally taken as unity [21]. Second, the absorbed dose at the medium surface is calculated from the absorbed dose at the water surface by the following relation [21]:

$$\dot{D}_{med,z=0} = C^{med}_w \dot{D}_{w,z=0}, \quad (2)$$

where C^{med}_w is the conversion factor to find the dose to medium from the dose to water. The C^{med}_w value for skin can be obtained from the Table 2 of TG-61 protocol if HVL value is specified.

Table 1
Average mass energy absorption coefficient ratios of water to air and free in air to convert air kerma to water kerma as a function of HVL (mm Al) or HVL (mm Cu).

First HVL		$[(\overline{\mu_{en}}/\rho)^{w}_{air}]_{air}$
(mm Al)	(mm Cu)	
0.03		1.047
0.04		1.047
0.05		1.046
0.06		1.046
0.08		1.044
0.10		1.044
0.12		1.043
0.15		1.041
0.2		1.039
0.3		1.035
0.4		1.031
0.5		1.028
0.6		1.026
0.8		1.022
1.0		1.020
1.2		1.018
1.5		1.017
2.0		1.018
3.0		1.021
4.0		1.025
5.0		1.029
6.0		1.034
8.0		1.045
	0.1	1.020
	0.2	1.028
	0.3	1.035
	0.4	1.043
	0.5	1.050
	0.6	1.056
	0.8	1.068
	1.0	1.076
	1.5	1.085
	2.0	1.089
	3.0	1.100
	4.0	1.106
	5.0	1.109

HVL, half value layer.
The data are from the study by Ma at el (Ref. [21]).

Consequently, using the Eqs. (1) and (2), the absorbed dose at the skin surface can be identified.

2.2.4. Percentage depth dose

Percentage depth dose (PDD) values of the EBT device were obtained by the following equation:

$$PDD = (D_d/D_{d_0}) \times 100, \quad (3)$$

where D_{d_0} is the absorbed dose at a reference depth of d_0 and D_d is the dose at a depth of interest. d_0 in this study was adjusted to 0 mm (skin surface). To measure the absorbed dose at different depth positions, polymethyl methacrylate (PMMA) plates with various thickness of 1–10 mm were used. The PMMA plates were placed between the surface applicator of the EBT device and the ionization chamber. D_d was measured with the ionization chamber by changing the thickness of the PMMA plates. To ensure full scattering, the ionization chamber was surrounded with 10-cm–thick PMMA.

2.3. RT experiments on skin cancer cells

Murine melanoma cells (B16F10) in 48-well plates were cultured for 1 day while being kept in Roswell Park Memorial Institute 1640 medium (Gibco/Invitrogen, Carlsbad, CA) at a density of 10,000 cells/mL. Single doses of 5 and 20 Gy using the EBT device were delivered to the treatment samples. To determine the number of cells in each sample, the cells were separated from the well using trypsin ethylenediaminetetraacetic acid and Dulbecco's phosphate-buffered saline solution. After the cells were detached from the vessel, the cell membranes were dyed with trypan blue solution. The quantification of the surviving cells was obtained by counting the number of cells with dyed membranes using an automated cell counter (LUNA; Logos Biosystems, Korea). The fractions of apoptotic cells was achieved by calculating the ratio of the surviving cell concentration of a treatment set to that of a control set. A set was composed of five samples.

2.4. In vivo animal RT experiments

In vivo RT in 5- to 7-week-old female C57BL/6 mice was performed using the EBT device. For the comparison, irradiation with a conventional 6 MeV linear accelerator (LINAC; Elekta, Stockholm, Sweden) was accomplished by placing mice in an acrylic chamber and using a bolus applied over a mass site with a source to skin distance of 100 cm. B16-F10 melanoma cell line was obtained for tumor growth from Japanese Collection of Research Bioresources cell bank. To establish tumor mass at the right thigh, mice were injected subcutaneously with 5×10^4 cultured melanoma cells. When the mass of tumor at the thigh reached 10 mm in diameter, mice were randomized into five groups: untreated control and four other groups irradiated at two different doses with two different radiation sources. Each group consisted of three mice. The mice bearing the tumors under deep anesthesia with Zoletil (10 mg/kg) were irradiated with both 50 kVp X-rays and 6 MeV electron beam at 5 and 20 Gy in a single fraction. Tumor growth delay method in which the time required for a tumor to grow to 1,000 cc after irradiation was measured and compared with that of a control group using the student *t* test. *In vivo* imaging system, which can take an image of animal tumorization, was used to check the antitumor activity. All animal experiments were performed under the institutional guidelines established by the Institutional Animal Care and Use Committee at Yonsei University (IACUC-2012-0177).

3. Results

3.1. Evaluations of the EBT device performance

3.1.1. X-ray spatial distribution

Fig. 2 displays the measurement results of the X-ray dose distributions generated from the 10-mm and 20-mm applicators. Flatness, symmetry, and penumbra of the X-rays derived from the dose distribution were 3.4%, 1.9%, and 0.23 mm for the 10-mm applicator and were 2.5%, 3.7%, and 0.23 mm for the 20-mm applicator, respectively. The accepted tolerance level of both flatness and symmetry for RT is 5% [17,22]. Moreover, penumbra value smaller than 1 mm is generally accepted for RT [14]. Therefore, these measured results reflect that the developed EBT device exhibits enough good performance for the application to the skin cancer treatment.

3.1.2. Half value layer

The HVL values of the X-rays generated from the 10-mm and 20-mm applicators were 0.13 mm Al and 0.1 mm Al, respectively. Note that HVL of 50 kVp X-rays typically ranges from 0.09 mm Al to 3.74 mm Al [21]. The central thickness of the conical-shaped flattening filter for the 10-mm applicator is 2.1 mm and that for the 20-mm applicator is 1.1 mm. Because lower energy X-rays are more attenuated while passing through a thicker filter, the average energy of X-rays generated from the 10-mm applicator becomes

Table 2
Free-in-air ratios of mass energy absorption coefficients of biological tissue to water for application in conjunction with the in-air method.

HVL		"Free-in-air" mass energy–absorption coefficient ratio of the specified tissues to water				
(mm Al)	(mm Cu)	ICRU 4-element soft tissue	ICRU striated muscle	ICRP lung	ICRP skin	ICRU compact bone
0.3		0.917	1.016	1.031	0.890	4.200
0.4		0.918	1.020	1.035	0.893	4.289
0.5		0.919	1.022	1.037	0.895	4.335
0.6		0.920	1.024	1.039	0.897	4.382
0.8		0.921	1.028	1.043	0.901	4.475
1.0		0.923	1.031	1.046	0.904	4.494
1.2		0.925	1.031	1.046	0.907	4.469
1.5		0.927	1.032	1.047	0.910	4.427
2.0		0.930	1.032	1.047	0.915	4.350
3.0		0.934	1.032	1.045	0.922	4.179
4.0		0.939	1.030	1.042	0.929	3.975
5.0		0.943	1.028	1.039	0.935	3.769
6.0		0.947	1.026	1.036	0.940	3.557
8.0		0.955	1.021	1.030	0.950	3.133
	0.1	0.934	1.032	1.045	0.921	4.209
	0.2	0.942	1.029	1.040	0.934	3.808
	0.3	0.947	1.026	1.036	0.940	3.561
	0.4	0.952	1.023	1.032	0.946	3.314
	0.5	0.956	1.020	1.029	0.952	3.068
	0.6	0.960	1.018	1.026	0.957	2.859
	0.8	0.964	1.015	1.022	0.961	2.657
	1.0	0.967	1.012	1.018	0.965	2.456
	1.5	0.975	1.006	1.009	0.975	1.952
	2.0	0.981	1.001	1.003	0.980	1.637
	3.0	0.986	0.996	0.997	0.985	1.280
	4.0	0.988	0.994	0.994	0.987	1.128
	5.0	0.990	0.992	0.992	0.989	1.026
	2.0	0.981	1.001	1.003	0.980	1.637
	3.0	0.986	0.996	0.997	0.985	1.280
	4.0	0.988	0.994	0.994	0.987	1.128
	5.0	0.990	0.992	0.992	0.989	1.026

The data are for SSD = 50 cm. These values can be used as C_w^{med}. The data are from the study by Ma at el (Ref. [21]).
ICRP, International Commission on Radiological Protection; ICRU, International Commission on Radiation Units; SSD, Source-Surface Distance.

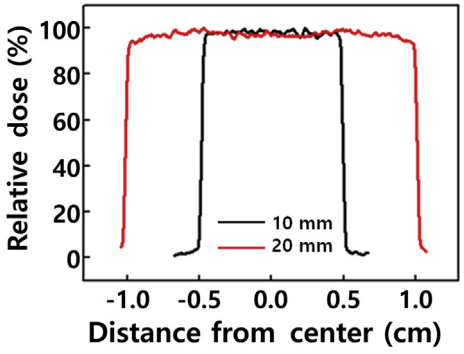

Fig. 2. Measured spatial dose distributions of the X-rays generated from the 10- and 20-mm applicator.

higher than that from the 20-mm applicator. As a consequence, the HVL value of the 10-mm applicator is larger than that of the 20-mm applicator.

3.1.3. Absorbed dose rate at the skin surface

The absorbed dose rate at the skin surface was determined from Eqs. (1), (2). The air kerma rates of the X-rays generated from the 10- and 20-mm applicators were 3.60 Gy/min and 5.61 Gy/min, respectively. B_w, $[(\overline{\mu}_{en}/\rho)^w_{air}]_{air}$, and C_w^{med} values identified from both the tables in TG-61 protocol and the measured HVL values were 1.043, 1.016, and 0.890 for the 10-mm applicator, and 1.044, 1.018, and 0.890 for the 20-mm applicator, respectively. Consequently, the absorbed dose rates at the skin surface calculated from these values were 3.39 Gy/min and 5.30 Gy/min for 10- and 20-mm applicators, respectively. The uncertainty of the derived absorbed dose rates is 3.6%, which comes from the uncertainties of the in-air method [21]. This uncertainty value is less than ± 5%, the maximum allowable uncertainty in a clinical situation [23].

3.1.4. Percentage depth dose

Fig. 3 shows the measurement results of the PDD profiles for the X-rays generated from the 10- and 20-mm applicator. Generally, the skin cancer is located at a depth of ~3 mm below the surface [24]. Because the measured PDD value at 3-mm depth is 34.56 % and the absorbed dose rate at the skin surface is 3.39 Gy/min for the 10-mm applicator, the absorbed dose rate at the skin cancer location is

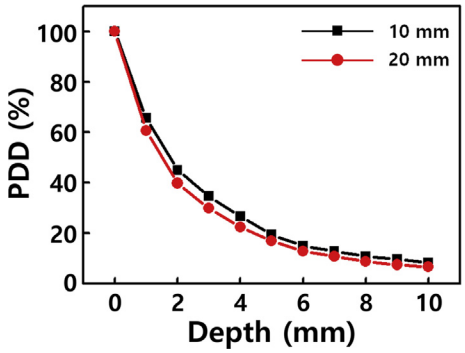

Fig. 3. Measured PDD curves of the X-rays generated from the 10- and 20-mm applicator.
PDD, percentage depth dose.

1.17 Gy/min, whereas the absorbed dose rate at the skin cancer location is 1.58 Gy/min for the 20-mm applicator, which is calculated from the PDD value of 29.82 % and the skin surface dose rate of 5.30 Gy/min.

3.2. *In vitro* and *in vivo* RT experiments

The experimental results on the apoptosis of the skin cancer cells after 5 Gy and 20 Gy X-ray exposure are shown in Fig. 4A and B. The rate of the surviving cell concentration was drastically reduced after the X-ray irradiation, and the fraction of the apoptotic cells increased with time after the irradiation. Higher dose of X-rays caused more significant apoptosis induction. As shown in Fig. 4C, 20 Gy dose induced 47% apoptotic fraction 1 day after, 71% 2 days after, and up to 79% 3 days after the irradiation, whereas, 5 Gy irradiation resulted in 61% of apoptotic fraction after 3 days.

In addition, luciferase activity shown in Fig. 5 significantly decreased in the irradiated groups compared with the untreated control group, without difference between the EBT- and the LINAC-treated groups. The growth delay curves display significant differences between the irradiated and control groups (Fig. 6). The mean time, which is defined as the time when the volume of the tumor reaches 1,000 cc, was 5.2 days in the control group. However, this value increased to 10.2 days and 14 days in the treated groups that were irradiated at 5 Gy and 20 Gy with the EBT device, respectively. In contrast, the mean time was 9.7 days and 13.2 days in the treated groups irradiated at 5 Gy and 20 Gy with the LINAC, respectively.

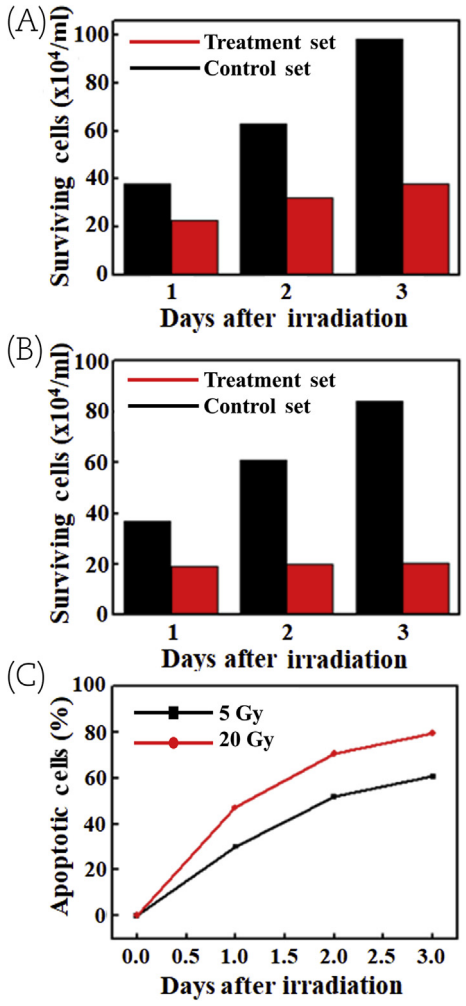

Fig. 4. *In vitro* results on the apoptosis of the skin cancer cells. (A) Concentration of surviving cancer cells for both 5 Gy-irradiated groups and control groups. (B) Concentration of surviving cancer cells for both 20 Gy-irradiated groups and control groups. (C) The fraction of apoptotic cells for both 5 Gy- and 20 Gy-irradiated groups.

4. Discussion

Skin cancers are typically located within a few mm below the surface even though deeper-seated tumors exist [24,25], and thus, superficial EBT can provide better treatment option than external RT because lower radiation energy of the EBT reduces the damage of deeper healthy skin cells.

Rapid radiation level falloff beyond the tumor depth due to lower radiation energy can minimize damage to healthy tissues; so, the treatment process is generally short and patient friendly. The treatments are also applicable to cosmetically sensitive areas such as eyelids, lips, nose, and ears. EBT also has a faster patient recovery time than protracted external radiation therapy [25].

Furthermore, less shielding requirement and lower device cost are also advantages of using EBT than using external RT. A few EBT devices for skin cancer treatment have been commercialized. Xoft device uses a miniature X-ray tube (diameter: 2.2 mm), but Esteya device does not use a miniature X-ray tube [14]. Intrabeam device has a narrow (diameter: 3.2 mm) and long (length: 10 cm) probe for X-ray production instead of using a miniature X-ray tube, and hence, a careful management is necessary to prevent bending of the probe [15]. The Xoft and the Intrabeam devices generate 50 kVp X-rays, whereas the Esteya device produces 69.5 kVp X-ray. Owing to the higher X-ray energy, the Esteya device has smaller depth-dose gradient (~7 %/mm) in the PDD profile than the Xoft device (~11 %/mm) when equipped with a surface applicator [14,17]. The dose gradient of the Intrabeam device is ~24 %/mm [16]. Meanwhile, the Xoft device requires water cooling to remove heat generated from both a thermionic electron source and an X-ray target, leading to the decrease in the X-ray dose rate and increase in the average X-ray energy after the passage through water. The Intrabeam device also uses a thermionic electron source, but no water cooling is required because electron beam current (40 μA) is far less than that (300 μA) of the Xoft device. This is the reason why the dose gradient of the Xoft device is smaller than that of the Intrabeam device even though the operating voltages of the two devices are the same.

Our novel EBT device uses a CNT-based miniature X-ray tube and is normally operated at 50 kVp [26]. Because heat is not generated from the CNT emitter, no water cooling is required for the operation of the device although electron beam current (250 μA) is comparable with that of the Xoft device. Moreover, the operating lifetime (>100 h) of the miniature X-ray tube is much longer than that (2.5 h) of the similar Xoft miniature X-ray tube. A dose gradient of ~24 %/mm below 3 mm in depth (Fig. 3) and a high dose rate of up to 5.30 Gy/min can be obtained from the EBT device. The dose gradient value is almost the same as that of the Intrabeam device. This high dose gradient results in a lower dose delivery to deeper healthy tissues, which is beneficial in terms of minimizing the damage to healthy tissues. In addition, because low-energy X-rays can be readily shielded by a thin lead sheet, a thin and soft lead plate with a hole in the shape corresponding to that of the tumor can be used. This allows X-rays to be irradiated only onto skin cancer cells while keeping the surrounding healthy areas unscathed.

The *in vitro* and *in vivo* RT studies show the effectiveness of the EBT device on skin cancer treatment. Apoptotic fraction of the skin cancer cells caused by the irradiation with the EBT device reached up to 80% after 3 days of the irradiation, indicating that a significant apoptosis occurred even after a single dose of the superficial X-ray irradiation. The luciferase activity shown in the *in vivo* imaging system was reduced in the irradiated group, demonstrating that EBT treatment enhances antitumor activities. In addition, the

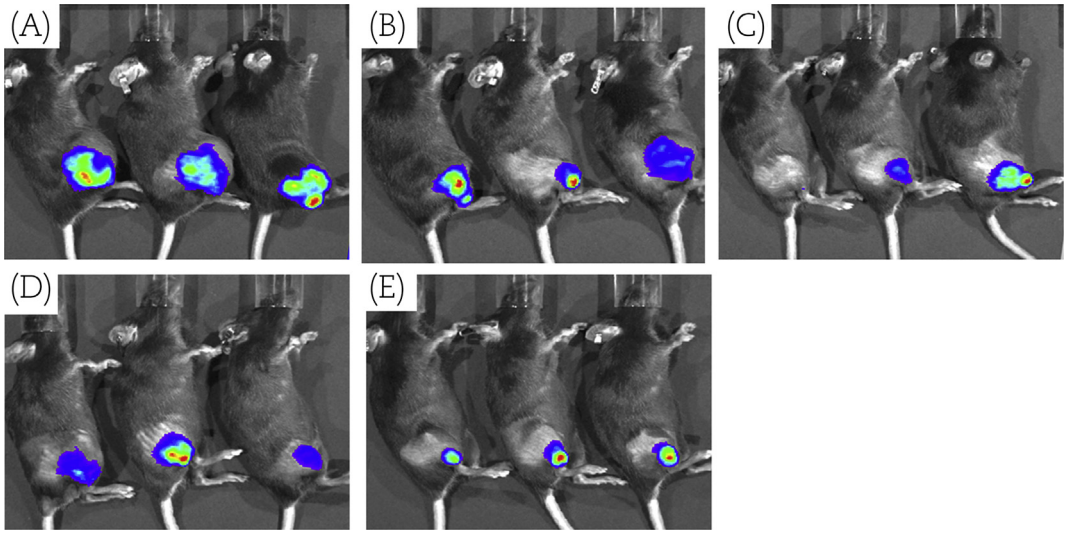

Fig. 5. Fluorescence signals obtained from the *in vivo* imaging system. (A) For the control group. (B) For the treatment group irradiated at 5 Gy with the LINAC. (C) For the treatment group irradiated at 20 Gy with the LINAC. (D) For the treatment group irradiated at 5 Gy with the EBT device. (E) For the treatment group irradiated at 20 Gy with the EBT device. EBT, electronic brachytherapy; LINAC, linear accelerator.

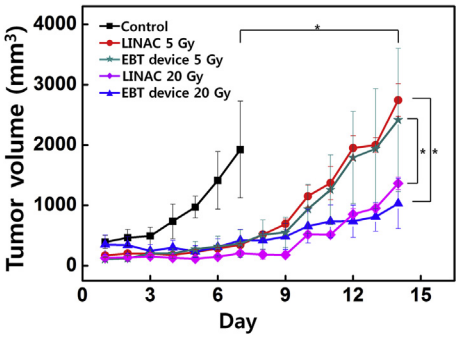

Fig. 6. Tumor growth delay curves for both the control group and treatment groups. * represents $p < 0.05$.
EBT, electronic brachytherapy; LINAC, linear accelerator.

results of the *in vivo* animal RT experiments show that the superficial X-rays significantly delay the tumor growth and that the EBT device has almost the same therapeutic effect as the LINAC. These preclinical data provide evidence for the practicality of EBT device application in the management of skin cancers. Further investigation to determine the optimal radiation dose to achieve optimal therapeutic effect without inducing toxicity is warranted.

5. Conclusions

A novel EBT device using a CNT-based miniature X-ray tube and a surface applicator has been developed for skin cancer treatment. The EBT device exhibited desirable dosimetric performance for skin cancer treatment and satisfied the accepted tolerance level for RT. Furthermore, the results of RT experiments on skin cancer cells and mice demonstrated the effectiveness of the EBT device on the skin cancer treatment, and these results show that the new EBT device has almost the same therapeutic effect as a conventional LINAC device. Therefore, we believe that the EBT device can be practically used for human skin cancer treatment in the near future after clinical verification.

Conflicts of interest

All authors have no conflicts of interest to declare.

Acknowledgment

This work was supported by the National Research Foundation of Korea (grant number NRF-2015M2A2A4A03045077), the Korean Health Industry Development Institute, funded by the Ministry of Health and Welfare, Republic of Korea (grant number: HI15C0638), and the Innopolis Foundation funded by the Korean Government (grant number ACC-2016-DDI-00793).

References

[1] H.W. Rogers, M.A. Weinstock, S.R. Feldman, B.M. Coldiron, Incidence estimate of nonmelanoma skin cancer (Keratinocyte Carcinomas) in the U.S. Population, 2012, JAMA Dermatol. 151 (2015) 1081–1086.
[2] R.S. Stern, Prevalence of a history of skin cancer in 2007: results of an incidence-based model, Arch. Dermatol. 146 (2010) 279–282.
[3] R.G. Freeman, J.M. Knox, C.L. Heaton, The treatment of skin cancer. A statistical study of 1,341 skin tumors comparing results obtained with irradiation, surgery, and curettage followed by electrodesiccation,, Cancer 17 (1964) 535–538.
[4] D.L. Shriner, D.K. McCoy, D.J. Goldberg, R.F. Wagner Jr., Mohs micrographic surgery, J. Am. Acad. Dermatol. 39 (1998) 79–97.
[5] N. Heidary, H. Naik, S. Burgin, Chemotherapeutic agents and the skin: an update, J. Am. Acad. Dermatol. 58 (2008) 545–570.
[6] E.G. Kuflik, A.A. Gage, The five-year cure rate achieved by cryosurgery for skin cancer,, J. Am. Acad. Dermatol. 24 (1991) 1002–1004.
[7] M.T. Wan, J.Y. Lin, Current evidence and applications of photodynamic therapy in dermatology, Clin. Cosmet. Investig. Dermatol. 7 (2014) 145–163.
[8] J. Locke, S. Karimpour, G. Young, M.A. Lockett, C.A. Perez, Radiotherapy for epithelial skin cancer, Int. J. Radiat. Oncol. Biol. Phys. 51 (2001) 748–755.
[9] W. Kwan, D. Wilson, V. Moravan, Radiotherapy for locally advanced basal cell and squamous cell carcinomas of the skin, Int. J. Radiat. Oncol. Biol. Phys. 60 (2004) 406–411.
[10] J.J. Silva, R.W. Tsang, T. Panzarella, W. Levin, W. Wells, Results of radiotherapy for epithelial skin cancer of the pinna: the Princess Margaret Hospital experience, 1982–1993, Int. J. Radiat. Oncol. Biol. Phys. 47 (2000) 451–459.
[11] M. Caccialanza, R. Piccinno, L. Kolesnikova, L. Gnecchi, Radiotherapy of skin carcinomas of the pinna: a study of 115 lesions in 108 patients, Int. J. Dermatol. 44 (2005) 513–517.
[12] M. El-Ashmawy, M. Uesaka, H. Iiijima, T. Imai, N.H. Quyet, Overall quality comparison of c-band and x-band medical linacs, in: The 14th Symposium on Accelerator Science and Technology, Tsukuba, Japan, 2003.
[13] F.F. Knapp, A. Dash, Radiopharmaceuticals for Therapy, Springer, 2016.
[14] Y. Rong, J.S. Welsh, New technology in high-dose-rate brachytherapy with surface applicators for non-melanoma skin cancer treatment: electronic miniature x-ray brachytherapy, in: Skin cancer overview, InTech, 2011.
[15] F. Schneider, H. Fuchs, F. Lorenz, et al., A novel device for intravaginal electronic brachytherapy, Int. J. Radiat. Oncol. Biol. Phys. 74 (2009) 1298–1305.
[16] S.C.P. Lam, Y. Xu, G. Ingram, L. Chong, et al., Dosimetric characteristics of intrabeam® flat and surface applicators, Transl. Cancer Res. 3 (2014) 106–111.

[17] T. Garcia-Martinez, J.P. Chan, J. Perez-Calatayud, F. Ballester, Dosimetric characteristics of a new unit for electronic skin brachytherapy, J. Contemp. Brachytherapy 6 (2014) 45–53.
[18] S.H. Heo, H.J. Kim, J.M. Ha, S.O. Cho, A vacuum-sealed miniature x-ray tube based on carbon nanotube field emitters, Nanoscale Res. Lett. 7 (2012) 258.
[19] J. Rassow, E. Klieber, Quality assurance procedures in radiotherapy–IEC specifications for equipment, Strahlenther. Onkol. Organ der Deutschen Rontgengesellschaft... [et al] 162 (1986) 496–502.
[20] A. Niroomand-Rad, C.R. Blackwell, B.M. Coursey, et al., Radiochromic film dosimetry: recommendations of aapm radiation therapy committee task group 55. American association of physicists in medicine, Med. Phys. 25 (1998) 2093–2115.
[21] C.M. Ma, C.W. Coffey, L.A. DeWerd, et al., Aapm protocol for 40-300 kv x-ray beam dosimetry in radiotherapy and radiobiology, Med. Phys. 28 (2001) 868–893.
[22] V.E. Kouloulias, P. Poortmans, C. Antypas, C. Kappas, P. Sandios, Field flatness and symmetry of photon beams: review of the current recommendations, Technol. Health Care Offic. J. Eur. Soc. Eng. Med. 11 (2003) 283–288.
[23] A. Brahme, Dosimetric precision requirements in radiation therapy, Acta Radiol. Oncol 23 (1984) 379–391.
[24] R. Ballester-Sanchez, O. Pons-Llanas, M. Llavador-Ros, et al., Depth determination of skin cancers treated with superficial brachytherapy: ultrasound vs. Histopathology, J. Contemp. Brachytherapy 6 (2015) 356–361.
[25] A. Bhatnagar, R. Patel, W.P. Werschler, R.I. Ceilley, R. Strimling, High-dose rate electronic brachytherapy: a nonsurgical treatment alternative for non-melanoma skin cancer, J. Clin. Aesthet Dermatol. 9 (2016) 16–22.
[26] H.J. Kim, H.Y. Kim, H. Saeed Raza, H.B. Park, S.O. Cho, An intraoral miniature X-ray tube based on carbon nanotubes for dental radiography, Nucl. Eng. Technol. 48 (2016) 799–804.